Interference Removal from Electromyography based on Independent Component Analysis

Yang Zheng and Xiaogang Hu

Abstract— **High-density surface electromyography (HD-EMG) provides detailed information about muscle activation. However, HD-EMG recordings can be interfered by motion artifacts and power line noise. In this study, an interference detection and removal method with minimal distortion of the EMG was developed based on independent component analysis (ICA). After the source separation, the independent components with power line noise were detected based on the spectra and were processed with notch filters. Components with motion artifacts were identified by analyzing the peak frequency of the spectrum, and motion artifacts were filtered with a high-pass filter and an amplitude thresholding method. The EMG signals were then reconstructed based on the processed source signals. The denoising performance was evaluated on both simulated and experimental EMG signals. The results showed that our method was significantly better than the digital filter method and the conventional ICA-based method where components with interferences were set to zero. Namely, our method showed a minimal distortion of the denoised EMG amplitude and frequency and a higher yield of decomposed motor units. Our interference detection and removal algorithm can be used as an effective preprocessing procedure, and can benefit macro level EMG analysis and micro level motor unit analysis.**

Index Terms— **Biosignal processing, Independent component analysis, Motion artifacts, Noise reduction, Power line noise**

I. Introduction

Surface electromyography (sEMG) is a noninvasive technique that can capture muscle activities with electrodes placed on the skin over muscle bellies [1]. It has been widely used in various purposes such as basic physiology, clinical diagnosis, rehabilitation, and ergonomics [2]. Recently, high-density sEMG (HD-EMG) can obtain a large number of EMG channels with closely spaced electrodes, and provide insight into the spatial distribution of myoelectric intensity from a wide muscle region. This information can help improve the identification of motor tasks [3, 4], reveal the distribution changes of muscle activation during stimulation-induced fatigue [5, 6], and help us understand muscle anatomy [7]. In addition, HD-EMG recordings also allow the extraction of motor unit (MU) activities non-invasively [8].

However, HD-EMG array typically have small electrode diameters (e.g., less than 3 mm), which are prone to changes in the electrode-electrolyte contact. As a result, the recordings can be contaminated with interference signals, including motion artifacts and large common mode interferences like power line noise. In order to reduce noise interference, several techniques have been developed. For example, Baratta et al. has developed a power line noise subtraction method based on the unrealistic assumption that the power line noise is constant throughout the recording [9]. Given the frequency characteristics of the motion artifact and the power line noise, a digital filter is commonly used [10, 11], despite the fact that the EMG signals are inevitably distorted due to spectral overlap. In contrast to the frequency filtering approach, recent efforts have tried to extract the time courses of artifact-related components. For instance, a moving median filter has been used to extract the artifact, and then subtracted it from the original signals [11]. More advanced noise component extraction technique, such as the empirical mode decomposition (EMD), has also been developed [12]. However, the EMD can fail to isolate artifacts when the artifacts contain oscillations overlapping with EMG signals.

Blind source separation techniques (e.g., independent component analysis (ICA) and canonical correlation analysis (CCA)) have provided an effective denoising tool by isolating individual source signals, including artifacts and the underlying physiological activities [13-17]. The ICA method estimates the different sources by maximizing the non-Gaussianity or mutual independence [18], while the CCA algorithm forces the sources to be mutually uncorrelated and maximally auto-correlated [19]. The CCA method was mainly used to reduce the white Gaussian noise [13, 15]. In addition, previous studies that utilized blind source separation have reduced the noise by setting the noise-related components to zero [13, 15]. There are several drawbacks in this approach. First, the noise component may still contain EMG activities. Second, simply setting the noise components to zero leads to a singular covariance matrix of the denoised EMG signals, which makes it impossible to perform spatial whitening as required by ICA-based EMG decomposition [20].

In our current study, an interference detection and removal method based on ICA was developed to remove motion artifacts and power line noise (the power line noise represents the interference at 60 Hz and higher order harmonics) from the HD-EMG signals. Instead of simply setting noise-related components to zero (termed ICA-Z method, Z means Zero) as in the conventional ICA approach, the power line noise in the components were detected based on their spectra and processed with notch filters. Components with motion artifacts

This study was supported by the National Science Foundation (Grant #: IIS-1637892) and the University Research Council.

Yang Zheng (email: yang1127@email.unc.edu) and Xiaogang Hu (email: xiaogang@unc.edu) are with the Joint Department of Biomedical Engineering at University of North Carolina-Chapel Hill and NC State University (correspondence e-mail: xiaogang@unc.edu)

were identified by analyzing the peak frequency of the spectra. Motion artifacts were then filtered with a high-pass filter and an amplitude thresholding method (termed ICA-FT method, FT means Filtering and Thresholding). Our approach was first evaluated on synthetic EMG signals, given that the ground-truth (clean EMG signals and MU activities) was known in simulated signals. We first calculated the difference (i.e., root mean squared error) between the denoised EMG and the clean EMG, and then quantified the number and accuracy of identifiable MU spike trains through EMG decomposition. The results showed that the ICA-FT method demonstrated a significant superiority to both the ICA-Z method and the conventional digital filter method, manifested as a smaller degree of distortion to the original EMG signals and a higher yield of decomposed MUs. Different denoising methods were then evaluated on experimental EMG recordings. The results showed that the ICA-FT method led to a smaller distortion of the amplitude and the median frequency of EMG signals.

II. METHODS

A. Noise detection and removal approach

The ICA-FT method included three steps (Fig. 1). The first step used a blind source separation technique, i.e. Infomax ICA [18] to extract individual independent components from the noise-contaminated EMG signals (termed noisy EMG in the subsequent text and figures). The second procedure involved the identification and processing of the components that contained artifacts. The last step reconstructed EMG signals with the processed components (termed ICA-FT-denoised EMG in the subsequent text and figures). The three steps were described in detail in the subsequent sections.

Noise separation. Infomax ICA is typically used to extract *n* mutually independent sources/components [18]. In our current study, some of the components mainly reflected the noise from *n* channels of the EMG signals.

Consider unknown *n* source signals $\mathbf{s}=[s_1,s_2,...,s_n]^T$, which are mutually independent. Each source is assumed to have moments of any order with a zero mean. The obtained signals $\mathbf{x}=[x_1,x_2,...,x_n]^{\mathrm{T}}$ can be considered as a linear mixture of the *n* source signals, $\mathbf{x}=\mathbf{A}\mathbf{s}$, where $\mathbf{A}\in\mathbf{R}^{n\times n}$ is an unknown non-singular mixing matrix. The process of Infomax ICA can be described as: given a set of signal mixtures $\mathbf{x}$ and a set of identical independent model cumulative distribution functions g, the unmixing matrix $\mathbf{W}$, which maximizes the joint entropy of the signals $\mathbf{y}=\mathrm{g}(\mathbf{c})$ ($\mathbf{y}=(1+e^{-\mathbf{c}})^{-1}$ in this study), are solved, where $\mathbf{c}=\mathbf{W}\mathbf{x}$ are the signals extracted by $\mathbf{W}$. Signals $\mathbf{y}$ are mutually independent. The Infomax ICA was implemented using a previously developed toolbox [21].

Component processing. The second step identified and processed the components with power line noise and motion artifacts. The goal was to reserve as much EMG information as possible after eliminating the noise. In order to eliminate the power line noise, the spectrum of individual components was estimated. If there was substantial spectral power at the frequencies of power line noise, notch filters (4th order Butterworth filter, zero-phase digital filtering, stop band: 57.5-62.5 Hz, 117.5-122.5 Hz, 177.5-182.5 Hz, and 237.5-242.5 Hz) were applied to the component (see Supplementary Material for details).

The procedure to eliminate motion artifacts involved two steps. The first step used a high-pass filter (Butterworth filter with an order of 4, zero-phase digital filtering) to remove the low-frequency activities if the frequency of peak spectral power of a component was smaller than 10 Hz, which was caused by motion artifacts. The second step further removed the residual of motion artifacts after the high-pass filtering. The basic idea was to locate the sporadic high peaks caused by the motion artifacts by characterizing the distribution of the peak values, and then set the samples related with motion artifacts to zero (see Supplementary Material for details).

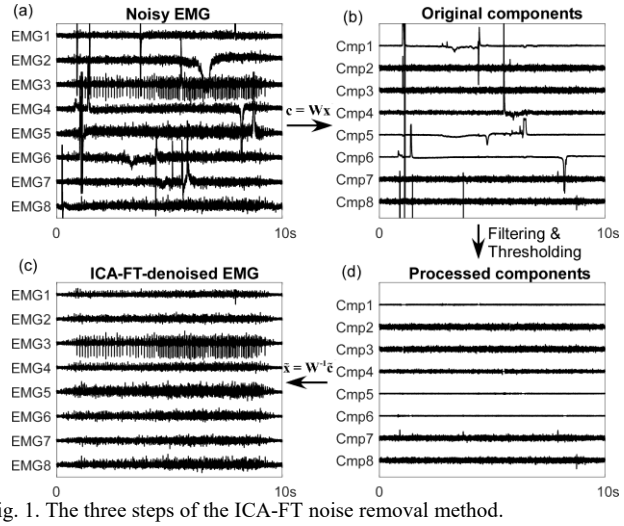

Fig. 1. The three steps of the ICA-FT noise removal method.

EMG signal reconstruction. The final step used the mixing matrix $\mathbf{W}^{-1}$ to obtain the ICA-FT-denoised EMG signals, $\tilde{\ }$, where $\tilde{\ }$ represented all the components, including the ones after processing. In the ICA-Z method, all components that were detected to contain artifacts through the ICA-FT procedure were set to zero and were used to reconstruct the ICA-Z-denoised EMG.

B. EMG and interference simulation

To simulate EMG signals, we first obtained the templates of realistic motion artifacts and MU action potentials (MUAPs) (see Supplementary Material for details) from experimental EMG signals as described in the next section. Briefly, the MUAP templates were estimated through a spike triggering averaging of the EMG signals [22]. MUAP templates of 104 MUs were obtained eventually. The motion artifact templates were also extracted from EMG signals obtained in the experiment using Infomax ICA [18]. Fig. 2a illustrates exemplar six of the total 50 motion artifact templates.

The synthetic clean EMG signals were simulated using a motoneuron recruitment model [23] and a convolution model [24]. The input to the motoneuron pool was an excitatory drive function representing the net synaptic input. The excitatory drive was normalized by the maximum drive level

corresponding to the maximum voluntary contraction (MVC). In the current study, the excitatory drive was a two-step trapezoid function that lasted for 10 seconds (Fig. 2b). The motoneuron pool contained a total of 120 neurons, and under the excitatory drive shown in Fig. 2b the actual number of recruited neurons was 91. In order to simulate the stochastic nature of motoneuron discharge times, each discharge timing was adjusted such that the inter-spike intervals were normally distributed with a 10% coefficient of variation and a mean value determined by the firing rate at an excitatory drive level.

The multi-channel EMG signals can be described as a convolutive mixture of a series of delta functions, which represent the discharge timings of the MUs [24, 25]:

$$x_i(k) = \sum_{j=1}^{m}\sum_{l=0}^{L-1} h_{ij}(l)s_j(k-l) + n_i(k)$$
$$i = 1,2,...,n; \quad k = 0,1,...,D_R \tag{1}$$

where $x_i(k)$ is the ith EMG channel, k is the discrete time, D_R is the total number of recorded data samples, m and n are the number of recruited MUs and EMG channels, respectively. $n_i(k)$ is the additive white noise at channel i, and its amplitude is set at a value corresponding to a signal-to-noise ratio (SNR) of 15 dB. The impulse responses in this convolutive mixture is the MUAP $h_{ij}(l)$ of the jth MU recorded at channel i, $s_j(k)$ is the MU discharge train of the jth MU, and L the MUAP duration. Five 10-second 64-channel clean EMG segments were simulated (Fig. 2c).

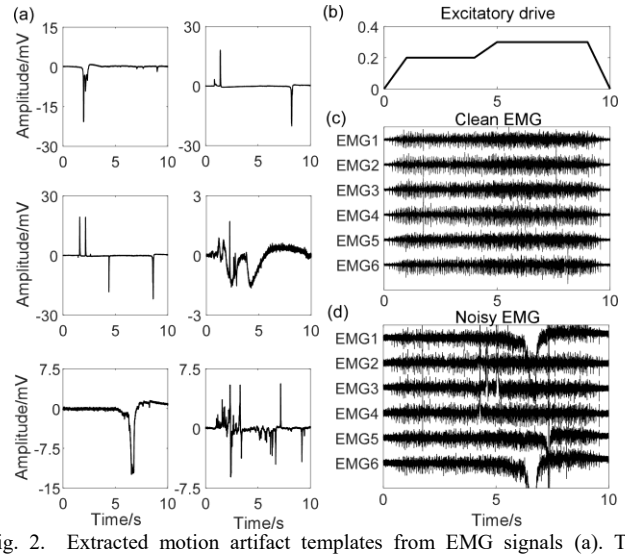

Fig. 2. Extracted motion artifact templates from EMG signals (a). The excitatory drive function as the input to the motoneuron pool (b). Six representative channels of EMG signals obtained with the convolutive mixture model (c). Six representative channels of EMG signals contaminated with motion artifacts and power line noise (SNR, 5 dB) (d).

Power line interference and motion artifacts were then added to obtain the noisy EMG (Fig. 2d). Multiple trials were simulated to investigate the performance of the noise removal method under different noise conditions.

The power line noise was added to the EMG as follows: a) Randomly select a clean EMG segment and estimate the average variance of the EMG signals across all channels. b) Based on the pre-set SNR (0 dB and 5 dB) of the power line noise, calculate the magnitude A_{60} of the power line noise (sinewave function) at 60 Hz. For higher order harmonics, the amplitude was calculated as $A_{60}(2/3)^{f_h/60}$, where f_h was the frequency of the harmonics. The amplitude of harmonics was determined according to previous studies [26, 27].

The motion artifacts were added to the EMG as follows: a) Randomly select N_{ma} motion artifacts from the motion artifact template pool. b) For a given motion artifact, randomly select 4 or 5 channels of EMG out of the 64 channels, and add the motion artifact to the selected channels. The saturation amplitude after added artifacts was set to ±5 mV. The number N_{ma} was 6 or 10, yielding a total of 24-30 or 40-50 EMG channels contaminated by the motion artifacts.

The denoising methods were first tested on individual types of interferences. For each SNR level or number of motion artifacts, ten trials were simulated. Then, both types of interferences were added to simulate noisy EMG signals. For each combination of the SNR and the number of motion artifacts, the procedures were repeated 10 times.

C. Experimental EMG acquisition

Eight healthy subjects (age: 20-34, one female and seven males) were recruited to perform a finger extension task. All subjects gave informed consent with protocols approved by the Institutional Review Board of the University of North Carolina at Chapel Hill.

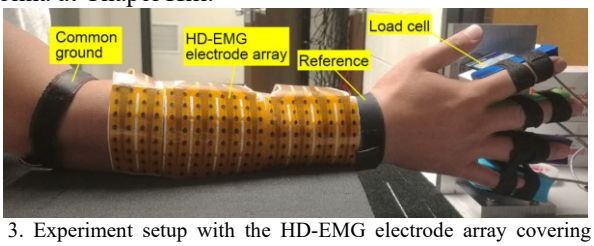

Fig. 3. Experiment setup with the HD-EMG electrode array covering the extensor digitorum communis muscles and four load cells measuring the extension force of individual fingers.

During the experiment, the subjects were seated comfortably in an arm chair. The index, middle, ring, and pinkie fingers were individually secured to four load cells (SM-200N, Interface, Scottsdale, AZ). The isometric extension forces were sampled at 1000 Hz. An 8×20 high-density EMG electrode array, with a 3-mm electrode diameter and a 10-mm inter-electrode distance covering the entire extensor digitorum communis, was used to record the muscle activities during finger extension (Fig. 3). Monopolar EMG signals were amplified with a gain of 1000 and a pass-band of 10-900 Hz, and were sampled at 2048 Hz via EMG-USB2+ (OT Bioelettronica, Torino, Italy).

The MVC of individual fingers were first measured. The main experiment involved a finger extension force tracking task of 5 minutes. Subjects were required to control the extension force of one finger to follow a pseudorandom force target, of which the level varied randomly between 20% and 40% MVC. The dynamic change in the force level can lead to changes of muscle geometry, and potentially can lead to motion artifacts. A total of six trials were obtained with two trials for each finger (index, middle, and ring).

D. Performance evaluation of simulated EMG

The performance of simulated EMG was evaluated from two aspects: 1) the degree of distortion of the denoised EMG measured as the root mean square error (RMSE) between the denoised EMG and the clean EMG, and 2) the number and the accuracy of the decomposed spike trains from the denoised EMG compared with that from the noise EMG. For comparison, both the ICA-Z method and the conventional method using high-pass and notch filters (termed Filter method) were used as control conditions. The notch filters, used in the ICA-FT method, were applied to all the EMG channels, and the high-pass filter was applied to channels with motion artifacts. The motion artifacts could have a wide frequency bandwidth overlapping with EMG signals. Therefore, there should be a trade-off between eliminating motion artifacts and maintaining EMG information. In order to identify the optimal cutoff frequency of the Filter method, eight cutoff frequencies were tested ranging from 25 - 200 Hz with a 25 Hz interval.

EMG distortion evaluation. The RMSE between the denoised EMG and the clean EMG was calculated as

$$R = \frac{1}{n}\sum_{i}^{n}\left(\frac{1}{T_s}\sum_{t}^{T_s}(x_i^c(t)-x_i^d(t))^2\right)^{1/2} \quad (2)$$

where $x_i^c(t)$ and $x_i^d(t)$ were the corresponding clean EMG and denoised EMG of the ith channel, n was the totally number of EMG channels, and T_s was the total number of data samples.

Extraction of MU spike train. MU spike trains were extracted from the simulated noisy EMG, the ICA-FT-denoised EMG, and the Filter-denoised EMG using an EMG decomposition method based on the FastICA algorithm [28, 29]. The *K-means* ++ algorithm was then used to identify the MU firing events from the source signal extracted from FastICA. Given that the same spike trains can be obtained through multiple iterations, 200 iterations were performed for each trial, in order to obtain as many spike trains as possible.

In order to quantify the number of the detected spike trains and the detection accuracy of the MUs, the true spike trains were compared with individual decomposed spike trains to determine whether they were identified. First, the common spikes were identified between a given true spike train and individual decomposed spike trains. Two spikes were considered common if the time delay between them was smaller than 2.5 ms. Then, the accuracy of the decomposed spike train was calculated as $A = N_{\text{com}} / (N_{\text{true}} + N_{\text{dec}}) \times 100\%$, where N_{com} was the number of common spikes, N_{true} and N_{dec} were the number of spike events in the true and decomposed spike train, respectively. For a given true spike train, the detection accuracies were calculated for all the decomposed spike trains, and the one with the highest accuracy was selected. If the highest accuracy was larger than an accuracy threshold (50%), the given true spike train was considered to be identified successfully. The total number of identified spike trains and the average detection accuracy across all identified spike trains were calculated for individual trials.

E. Performance evaluation of experimental EMG

In order to evaluate the performance of different denoising methods in realistic applications, the amplitude (root mean square (RMS)) and median frequency of experimental EMG signals were investigated before and after different denoising methods. Sixty eight (9±3 segments per subject) 10-second segments were manually selected from the experimental EMG during constant contraction levels. Each segment contained 64 channels based on the EMG amplitude and the location of the motion artifacts. As a result, the motion artifacts were either involved in the first 5 seconds (33 segments and 28±4 channels contaminated with motion artifacts) or the last 5 seconds (35 segments and 27±5 channels contaminated with motion artifacts). The different denoising methods were only performed on the 5-second portions with noise. We then calculated the RMS and the median frequency of individual channels from both the denoised portion and the clean portion. The absolute difference of the RMS (or median frequency) between the denoised and clean portions was calculated and averaged across the channels with motion artifacts. The difference of RMS (or median frequency) was also averaged across the channels without motion artifacts, in order to quantify how the denoising procedures distorted the EMG signals. Lastly, before the denoising procedures, the difference of RMS and median frequency of the EMG channels without motion artifacts was also calculated as a ground-truth. Since the contraction level was constant and the EMG activity was relatively stable, we expected that the difference in the RMS and the median frequency would be small, if the denoising procedures only removed motion artifacts with minimal distortion of the EMG signals.

F. Statistical analysis

All the evaluation variables were analyzed with a repeated measures ANOVA, and a post-hoc pairwise comparison was performed when necessary, using the Holm–Bonferroni correction method. A significant level was set to $\alpha = 0.05$ for all the testing.

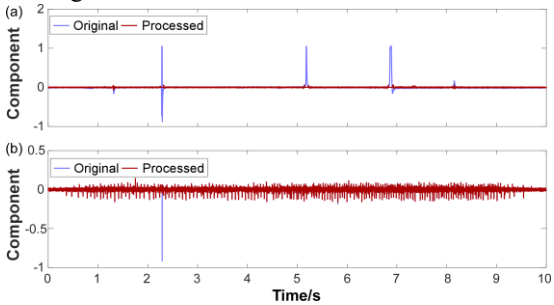

Fig. 4. Two representative independent components from a single trial, with one containing mainly motion artifacts (a) and one containing both motion artifacts and EMG activities (b). The corresponding results after the ICA-FT denoising procedure are overlaid with the original noisy components.

III. Results

A. EMG distortion evaluation

Fig. 4 illustrates two representative components extracted from a noisy EMG segment. The component shown in Fig. 4a contained mainly motion artifacts, which were eliminated through the ICA-FT procedure. The component shown in Fig. 4b contained both motion artifacts and EMG spikes. The ICA-FT procedures eliminated the motion artifact and retained the EMG activities. However, the conventional ICA-Z method would remove both motion artifacts and EMG activities by setting the component to zero.

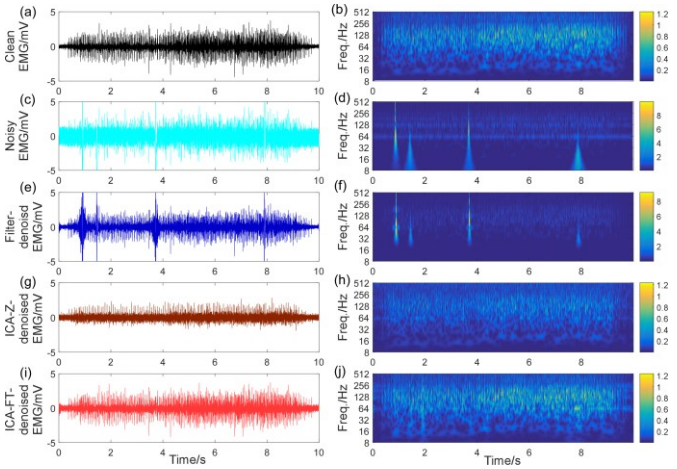

Fig. 5. The clean EMG (a), the noisy EMG (c), the Filter-denoised EMG (e), the ICA-Z-denoised EMG (g), the ICA-FT-denoised EMG (i), and their corresponding time-frequency spectrum (b), (d), (f), (h), and (j), respectively.

Fig. 5 illustrates the clean EMG from one representative channel (a), and the corresponding noisy EMG (c), the Filter-denoised EMG (50 Hz high-pass; 60 Hz, 120 Hz, 180 Hz, and 240 Hz notch) (e), the ICA-Z-denoised EMG (g) and the ICA-FT-denoised EMG (i). All noise reduction methods can effectively reduce the power line noise as shown in the time-frequency spectrum in Fig. 5f, 5h, and 5j. Motion artifacts had wide frequency bandwidths overlapping with the EMG signals (Fig. 5d). When a high-pass filter was used, the high-frequency components of the motion artifacts cannot be removed completely (Fig. 5f). In contrast, motion artifacts were not evident from the ICA-Z-denoised EMG and the ICA-FT-denoised EMG. However, the ICA-Z method also eliminated EMG activities, as shown from the decreased amplitude and the changed time-frequency spectrum of the ICA-Z-denoised EMG compared with the clean EMG.

When the noisy EMG only contained power line noise, the RMSE of different denoised EMG are illustrated in Fig. 6a. The ANOVA results showed that there was significant differences between the three types of EMG for both SNR levels (SNR, 5 dB: $F(2,18)=164.75$, $p<0.0001$; SNR, 0 dB: $F(2,18)=228.04$, $p<0.0001$). Further post-hoc test showed that the RMSE of the ICA-FT-denoised EMG was significantly smaller than that of the other two types of EMG ($p<0.0001$), and the RMSE of the ICA-Z-denoised EMG was significantly larger than that of the Filter-denoised EMG ($p<0.0001$).

When the noisy EMG only contained motion artifacts (Fig. 6b), the RMSE of the high-pass filter approach first decreased and then increased as the cutoff frequency increased from 25 Hz to 200 Hz, and the smallest RMSE was obtained with a cutoff frequency around 50 to 75 Hz. Therefore, the RMSE values obtained with the cutoff frequencies of 50 Hz and 75 Hz were compared with the RMSE of the ICA-denoised EMG. The ANOVA results showed that there was significant differences between the four types of EMG (ICA-FT-denoised, ICA-Z-denoised, Filter-denoised at 50 and 75 Hz) for both noise conditions (number of motion artifact (# MA), 6: $F(3,27)=39.48$, $p<0.0001$; # MA, 10: $F(3,27)=39.10$, $p<0.0001$). Further post-hoc test showed that the RMSE of the ICA-FT-denoised EMG was significantly smaller compared with the ICA-Z-denoised EMG and both Filter-denoised EMG signals ($p<0.0001$). There was no significant difference between the ICA-Z-denoised EMG and the Filter-denoised EMG ($p>0.1$).

When the noisy EMG signals contained both power line noise and motion artifacts (Fig. 6c), similar results were observed as in Fig. 6b. The RMSE values obtained with the

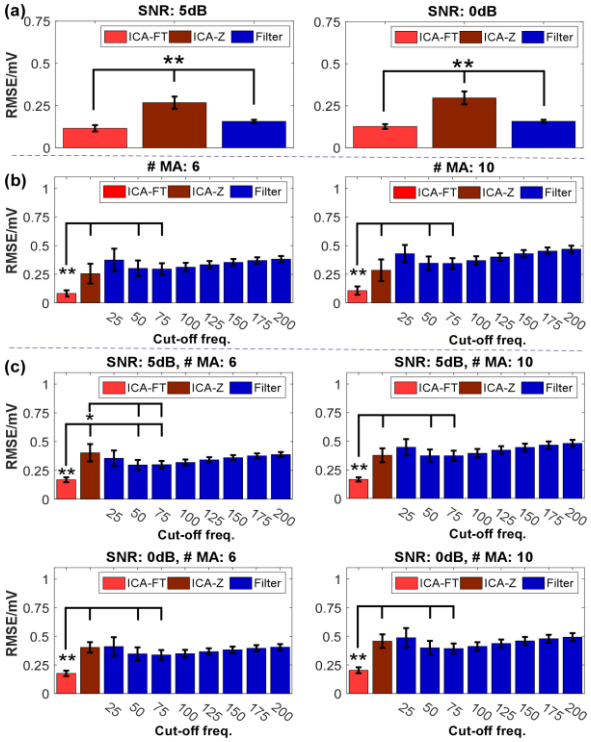

Fig. 6. The average root mean square error (RMSE) between the clean EMG and the denoised EMG obtained with the different denoising methods. The noisy EMG only contained power line noise (a). The noisy EMG only contained motion artifacts (b). The noisy EMG was contaminated with both power line noise and motion artifacts (c).The error bar represents standard error. *, $p<0.05$, **, $p<0.0001$.

cutoff frequencies of 50 and 75 Hz were compared with the RMSE of the ICA-FT and ICA-Z conditions. The ANOVA results showed that there was significant differences between the four types of EMG (ICA-FT-denoised, ICA-Z-denoised, Filter-denoised at 50 and 75 Hz) for all the noise conditions (SNR, 5 dB, # MA, 6: $F(3,27)=46.25$, $p<0.0001$; SNR, 5 dB, # MA, 10: $F(3,27)=101.75$, $p<0.0001$; SNR, 0 dB, # MA, 6: $F(3,27)=64.48$, $p<0.0001$; SNR, 0 dB, # MA, 10: $F(3,27)=96.77$, $p<0.0001$). Further post-hoc showed that the RMSE of the ICA-FT-denoised EMG was significantly smaller compared with the other three types of EMG for all the noise conditions ($p<0.0001$). In addition, the RMSE of the ICA-Z-denoised EMG was significantly larger than that of the

Filter-denoised EMG when SNR=5 dB and # MA=6 ($p<0.05$).

B. *Evaluation of MU spike trains*

Spike trains were extracted via EMG decomposition algorithms using the ICA-FT-denoised EMG, the Filter-denoised EMG (50 Hz high-pass and notch filters) and the raw noisy EMG. The decomposition results of an example trial are shown in the Supplementary Material. The ICA-Z-denoised EMG was not used because the covariance matrix of the denoised EMG was singular, and whitening procedure cannot be performed.

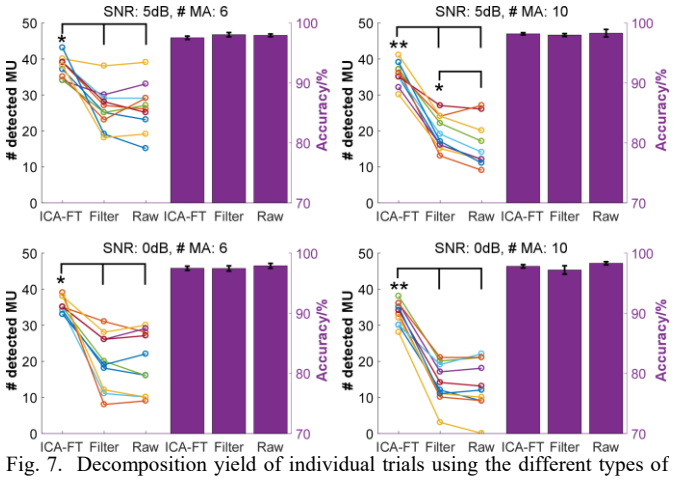

Fig. 7. Decomposition yield of individual trials using the different types of EMG signals (left y axis). The average decomposition accuracy using different types of EMG (right y axis). The error bar represents standard error. *, $p<0.05$, **, $p<0.0001$.

The decomposition yield and accuracy of all the conditions are summarized in Fig. 7. The ANOVA showed that the types of EMG (ICA-FT-denoised, Filter-denoised and raw noisy EMG) had significant influence on the decomposition yield for all the conditions (SNR, 5 dB, # MA, 6: $F(2,18)=21.85$, $p<0.0001$; SNR, 5 dB, # MA, 10: $F(2,18)=94.73$, $p<0.0001$; SNR, 0 dB, # MA, 6: $F(2,18)=30.68$, $p<0.0001$; SNR, 0 dB, # MA, 10: $F(2,18)=146.21$, $p<0.0001$). Further post-hoc test showed that the decomposition yield of the ICA-FT-denoised EMG was significantly larger than that of the Filter-denoised EMG or raw noisy EMG for all the noise conditions (# MA, 6: $p<0.05$; # MA, 10: $p<0.0001$). The filter method significantly increase the decomposition yield compared with that using the raw noisy EMG only when the SNR was 5 dB and the number of motion artifacts was 10 ($p<0.05$). Even though the decomposition yield between different types of EMG differed significantly, the decomposition accuracy showed no significant difference in any conditions (SNR, 5 dB, # MA, 6: $F(2,18)=0.82$, $p=0.45$; SNR, 5 dB, # MA, 10: $F(2,18)=0.21$, $p=0.81$; SNR, 0 dB, # MA, 6: $F(2,18)=0.42$, $p=0.67$; SNR, 0 dB, # MA, 10: $F(2,18)=1.55$, $p=0.24$).

C. *Evaluation of experimental EMG*

The differences in RMS or median frequency across all subjects are illustrated in Fig. 8. Regarding the difference in median frequency from channels with motion artifacts (Fig. 8a), the ANOVA showed that the different denoising methods had a significant effect ($F(3,21)=46.1$, $p<0.0001$). Post-hoc test showed a significant difference between any two types of EMG ($p<0.05$). The ANOVA showed that the different denoising methods also had a significant effect ($F(2,14)=25.4$, $p<0.0001$) on the channels without motion artifacts (Fig. 8b). Post-hoc test indicated that the difference in median frequency of the ICA-Z-denoised EMG was significantly larger than that of the ICA-FT-denoised EMG and the ground-truth ($p<0.05$), while there was no significant difference between the ICA-FT-denoised and the ground-truth ($p>0.05$).

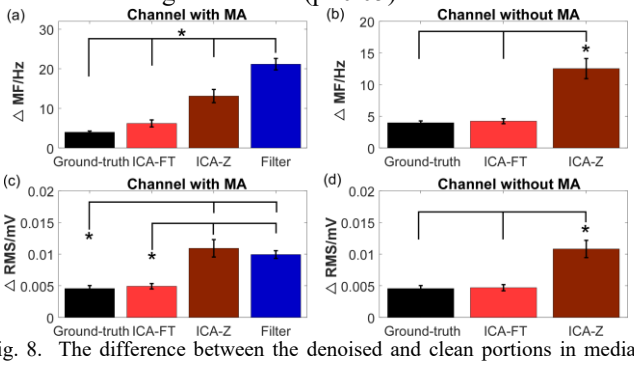

Fig. 8. The difference between the denoised and clean portions in median frequency of channels with motion artifacts (a) and without motion artifacts (b). The difference in RMS of channels with motion artifacts (c) and without motion artifacts (d). The error bar represents the standard error. *, $p<0.05$.

The different denoising methods also significantly influenced the difference in RMS of channels with motion artifacts as shown in Fig. 8c ($F(3,21)=19.3$, $p<0.0001$). Post-hoc test showed that the difference in RMS of the ground-truth and the ICA-FT-denoised EMG was significantly smaller compared with the ICA-Z-denoised EMG and the Filter-denoised EMG ($p<0.05$). However, there was no significant difference between the ground-truth and the ICA-FT-denoised EMG ($p>0.05$). Considering the difference in RMS of the channels without motion artifacts (Fig. 8d), there were significant differences between denoising methods ($F(2,14)=21.6$, $p<0.0001$). Further post-hoc test showed that the difference in RMS of the ICA-Z-denoised EMG was significantly larger compared with the ground-truth and the ICA-FT-denoised EMG, and there was no significant difference between the ICA-FT-denoised EMG and the ground-truth ($p>0.05$).

IV. Discussion

In this study, an ICA-based denoising method was developed to automatically detect and remove motion artifacts and power line noise from HD-EMG signals. The denoising performance was first assessed using simulated EMG. Our results showed that the ICA-FT-denoised EMG had a significantly smaller RMSE compared with the Filter-denoised EMG and the ICA-Z-denoised EMG, which demonstrated a lower degree of EMG distortion. The ICA-FT method also significantly increased the yield of EMG decomposition even if the EMG signals were severely contaminated with motion artifacts and power line noise, in comparison with conventional methods. The different denoising methods were then evaluated on experimental EMG recordings. The ICA-FT method again showed minimal distortion of the EMG signals (RMS and median frequency), compared with the ICA-Z method and the conventional filter method. Overall, our

findings demonstrated high performance of the ICA-FT denoising method for HD-EMG signal preprocessing. The method can benefit subsequent signal processing either focused on the macro level EMG features or on the micro level MU discharge properties.

The evaluation of EMG distortion reveals the advantage of our method on recovering the underlying EMG activities, compared with the conventional filtering method and the ICA-Z method. Power line noise generally contaminates all channels during data recording, and notch filters are applied to all channels. Since the frequency of power line noise is within the frequency bandwidth of EMG activities, the notch filtering will inevitably eliminate some EMG information. As for the removal of motion artifacts, the conventional filtering method is not able to remove all the motion artifacts because of overlapping frequency bandwidths between the motion artifacts and the EMG signals. The cut-off frequency of high-pass filters is typically limited to a low frequency range to reduce the impact on the actual EMG activities. As a result, a low cut-off frequency can still leave substantial residuals of the motion artifacts in EMG recordings. Even though the conventional ICA-Z method [13, 15] can extract the interferences from EMG activities, it is possible that the components containing interferences still involved EMG activities, as shown in our results. Simply setting the components to zero would eliminate EMG activities, resulting in distortion of the denoised EMG. In contrast, in the ICA-FT denoising method, filtering procedures were performed only on the components that involved substantial power line noise and/or motion artifact. The EMG information in other components was not distorted. Thus, when the components were mapped back to the EMG channel space, the residual of the noise had little influence on the underlying EMG signals.

Macro features (e.g., RMS and median frequency) are typically extracted from EMG recordings in different myoelectric-based applications such as pattern recognition [30, 31]. Motion artifacts can substantially distort the RMS and median frequency estimation. In our current study, the effect of different denoising methods on the RMS and median frequency estimation was investigated using experimental EMG recordings. Different denoising methods were applied to the noise-contaminated portion of EMG signals. The difference of RMS (or median frequency) between the denoised portion and the clean portion was used to quantify the denoising effect. The results showed that the ICA-FT-denoised EMG had smaller differences in the RMS or the median frequency, compared with the Filter-denoised EMG and the ICA-Z-denoised EMG. The results demonstrated that the ICA-FT method had the smallest EMG distortion while removing the interference, compared with other methods.

Micro features, involving MU decomposition of EMG signals, were also evaluated. The decomposition yield of the ICA-FT-denoised EMG significantly increased, in comparison with both the yields from the Filter-denoised EMG and the noisy EMG. One possible explanation was that the FastICA iterations used for the EMG decomposition frequently converged to the motion artifacts. Since the motion artifacts cannot be eliminated completely through the filtering method, the number of detected MUs using the Filter-denoised EMG had no significant difference compared with the raw noisy EMG. In some trials, the number of detected MUs using the Filter-denoised EMG was even smaller than that using the raw noisy EMG, possibly because the digital filter procedure also removed substantial EMG information.

On the other hand, the detection accuracy of spike trains had no significant difference among the different types of EMG signals. It was possible that the motion artifacts were independent of the MU firing spikes, and the MU spike trains can be extracted from the EMG independently. It was also possible that the motion artifacts generally lasted for a short period. If a MU can be detected, it only affected several spike events near the motion artifacts, which may not substantially affect the overall detection accuracy. The average detection accuracy using the ICA-FT-denoised EMG was slightly lower (by less than 1.0%) compared with the other two types of EMG. It was likely that some detected MUs with the ICA-FT-denoised EMG had lower detection accuracy, because the algorithm had higher chance converging to the spike trains with low SNRs, which led to a lower average decomposition accuracy across all detected MUs. Nevertheless, considering the benefit of significantly increased yield, the effect of slightly decreased accuracy was negligible. A high detection accuracy (>95%) was obtained regardless the types of EMG signals. The consistently high accuracy can arise from the fact that a relatively low amplitude of white Gaussian noise (15 dB SNR) was added in the convolution mixing model, which can affect the detection accuracy of spike trains.

One limitation of the ICA-FT denoising method is that the white Gaussian noise is not varied and removed, mainly because the amplitude of white Gaussian noise is small with the development of advanced amplifier techniques. Nevertheless, the removal of white Gaussian noise need to be addressed in further studies by combining ICA with CCA, which is more effective in isolating white Gaussian noise.

V. Conclusions

In general, our results showed that the ICA-FT noise detection and removal method can effectively eliminate motion artifacts and power line noise from HD-EMG recordings without interfering the EMG signals. The major difference of our developed method compared with previous studies based on the blind source separation techniques lies in the processing of noise related independent components. Notch filters at power line frequency were applied to the components with substantial power line noise. The motion artifacts were removed by combining a high-pass filtering and a motion artifact suppression procedure. These procedures allowed us to just focus on noise activities, and retain as much EMG information as possible. Our results showed that the ICA-FT denoising method can significantly improve the denoising performance compared with the conventional digital filter and ICA-Z methods, with minimal distortion of the denoised EMG. Our developed denoising algorithm can be used as a preprocessing procedure of HD-EMG recordings

that can benefit different types of applications from macro level EMG analysis to micro level MU analysis.

REFERENCES

[1] H. J. Hermens, B. Freriks, C. Disselhorst-Klug, and G. Rau, "Development of recommendations for SEMG sensors and sensor placement procedures," *Journal of electromyography and Kinesiology,* vol. 10, no. 5, pp. 361-374, 2000.

[2] M. Barbero, R. Merletti, and A. Rainoldi, *Atlas of muscle innervation zones: understanding surface electromyography and its applications*. Springer Science & Business Media, 2012.

[3] M. Jordanic, M. Rojas-Martínez, M. A. Mañanas, and J. F. Alonso, "Spatial distribution of HD-EMG improves identification of task and force in patients with incomplete spinal cord injury," *Journal of neuroengineering and rehabilitation,* vol. 13, no. 1, p. 41, 2016.

[4] M. Rojas-Martínez, M. Mañanas, J. Alonso, and R. Merletti, "Identification of isometric contractions based on High Density EMG maps," *Journal of electromyography and kinesiology,* vol. 23, no. 1, pp. 33-42, 2013.

[5] Y. Zheng and X. Hu, "Improved muscle activation using proximal nerve stimulation with subthreshold current pulses at kilohertz-frequency," *Journal of neural engineering,* vol. 15, no. 4, p. 046001, 2018.

[6] Y. Zheng and X. Hu, "Reduced muscle fatigue using kilohertz-frequency subthreshold stimulation of the proximal nerve," *Journal of neural engineering,* vol. 15, no. 6, p. 066010, 2018.

[7] B. G. Lapatki, R. Oostenveld, J. P. Van Dijk, I. E. Jonas, M. J. Zwarts, and D. F. Stegeman, "Topographical characteristics of motor units of the lower facial musculature revealed by means of high-density surface EMG," *Journal of neurophysiology,* vol. 95, no. 1, pp. 342-354, 2006.

[8] M. Chen and P. Zhou, "A novel framework based on FastICA for high density surface EMG decomposition," *IEEE Transactions on Neural Systems and Rehabilitation Engineering,* vol. 24, no. 1, pp. 117-127, 2016.

[9] R. Baratta, M. Solomonow, B.-H. Zhou, and M. Zhu, "Methods to reduce the variability of EMG power spectrum estimates," *Journal of Electromyography and Kinesiology,* vol. 8, no. 5, pp. 279-285, 1998.

[10] R. G. Mello, L. F. Oliveira, and J. Nadal, "Digital Butterworth filter for subtracting noise from low magnitude surface electromyogram," *Computer methods and programs in biomedicine,* vol. 87, no. 1, pp. 28-35, 2007.

[11] S. Conforto, T. D'Alessio, and S. Pignatelli, "Optimal rejection of movement artefacts from myoelectric signals by means of a wavelet filtering procedure," *Journal of Electromyography and Kinesiology,* vol. 9, no. 1, pp. 47-57, 1999.

[12] H. Liang, Q.-H. Lin, and J. Chen, "Application of the empirical mode decomposition to the analysis of esophageal manometric data in gastroesophageal reflux disease," *IEEE Transactions on biomedical engineering,* vol. 52, no. 10, pp. 1692-1701, 2005.

[13] M. Al Harrach *et al.*, "Denoising of HD-sEMG signals using canonical correlation analysis," *Medical & biological engineering & computing,* vol. 55, no. 3, pp. 375-388, 2017.

[14] K. T. Sweeney, S. F. McLoone, and T. E. Ward, "The use of ensemble empirical mode decomposition with canonical correlation analysis as a novel artifact removal technique," *IEEE transactions on biomedical engineering,* vol. 60, no. 1, pp. 97-105, 2013.

[15] M. Hassan, S. Boudaoud, J. Terrien, B. Karlsson, and C. Marque, "Combination of canonical correlation analysis and empirical mode decomposition applied to denoising the labor electrohysterogram," *IEEE Transactions on Biomedical Engineering,* vol. 58, no. 9, pp. 2441-2447, 2011.

[16] T.-P. Jung, S. Makeig, M. Westerfield, J. Townsend, E. Courchesne, and T. J. Sejnowski, "Removal of eye activity artifacts from visual event-related potentials in normal and clinical subjects," *Clinical Neurophysiology,* vol. 111, no. 10, pp. 1745-1758, 2000.

[17] T.-P. Jung *et al.*, "Removing electroencephalographic artifacts by blind source separation," *Psychophysiology,* vol. 37, no. 2, pp. 163-178, 2000.

[18] A. J. Bell and T. J. Sejnowski, "An information-maximization approach to blind separation and blind deconvolution," *Neural computation,* vol. 7, no. 6, pp. 1004-1034, 1995.

[19] W. De Clercq, A. Vergult, B. Vanrumste, W. Van Paesschen, and S. Van Huffel, "Canonical correlation analysis applied to remove muscle artifacts from the electroencephalogram," *IEEE transactions on Biomedical Engineering,* vol. 53, no. 12, pp. 2583-2587, 2006.

[20] A. Belouchrani, K. Abed-Meraim, J.-F. Cardoso, and E. Moulines, "A blind source separation technique using second-order statistics," *IEEE Transactions on signal processing,* vol. 45, no. 2, pp. 434-444, 1997.

[21] A. Delorme and S. Makeig, "EEGLAB: an open source toolbox for analysis of single-trial EEG dynamics including independent component analysis," *Journal of neuroscience methods,* vol. 134, no. 1, pp. 9-21, 2004.

[22] X. Hu, W. Z. Rymer, and N. L. Suresh, "Motor unit pool organization examined via spike-triggered averaging of the surface electromyogram," *Journal of neurophysiology,* vol. 110, no. 5, pp. 1205-1220, 2012.

[23] A. J. Fuglevand, D. A. Winter, and A. E. Patla, "Models of recruitment and rate coding organization in motor-unit pools," *Journal of neurophysiology,* vol. 70, no. 6, pp. 2470-2488, 1993.

[24] R. S. Lefever, A. P. Xenakis, and C. J. De Luca, "A procedure for decomposing the myoelectric signal into its constituent action potentials-part II: execution and test for accuracy," *IEEE transactions on biomedical engineering,* no. 3, pp. 158-164, 1982.

[25] F. Negro, S. Muceli, A. M. Castronovo, A. Holobar, and D. Farina, "Multi-channel intramuscular and surface EMG decomposition by convolutive blind source separation," *Journal of neural engineering,* vol. 13, no. 2, p. 026027, 2016.

[26] M. R. Keshtkaran and Z. Yang, "A fast, robust algorithm for power line interference cancellation in neural recording," *Journal of neural engineering,* vol. 11, no. 2, p. 026017, 2014.

[27] M. R. Keshtkaran and Z. Yang, "Power line interference cancellation in in-vivo neural recording," in *2012 Annual International Conference of the IEEE Engineering in Medicine and Biology Society*, 2012, pp. 5214-5217: IEEE.

[28] H. Nakamura, M. Yoshida, M. Kotani, K. Akazawa, and T. Moritani, "The application of independent component analysis to the multi-channel surface electromyographic signals for separation of motor unit action potential trains: part II—modelling interpretation," *Journal of Electromyography and Kinesiology,* vol. 14, no. 4, pp. 433-441, 2004.

[29] H. Nakamura, M. Yoshida, M. Kotani, K. Akazawa, and T. Moritani, "The application of independent component analysis to the multi-channel surface electromyographic signals for separation of motor unit action potential trains: Part I—Measuring techniques," *Journal of Electromyography and Kinesiology,* vol. 14, no. 4, pp. 423-432, 2004.

[30] N. Nazmi, M. Abdul Rahman, S.-I. Yamamoto, S. Ahmad, H. Zamzuri, and S. Mazlan, "A review of classification techniques of EMG signals during isotonic and isometric contractions," *Sensors,* vol. 16, no. 8, p. 1304, 2016.

[31] A. Phinyomark, C. Limsakul, and P. Phukpattaranont, "A novel feature extraction for robust EMG pattern recognition," *arXiv preprint arXiv:0912.3973,* 2009.